Science of the Total Environment 905 (2023) 167173

Contents lists available at ScienceDirect

Science of the Total Environment

journal homepage: www.elsevier.com/locate/scitotenv

Effects of near-bed turbulence on microplastics fate and transport in streams

Huan Yang, Hosein Foroutan *

Department of Civil and Environmental Engineering, Virginia Tech, Blacksburg, VA 24061, United States

HIGHLIGHTS

- Turbulent hyporheic flow affects the fate and transport of in-stream microplastics.
- Small and buoyant microplastics are more susceptible to turbulent hyporheic flow.
- High flow, permeable bed, and mounded bedform enhance microplastics transport.

GRAPHICAL ABSTRACT

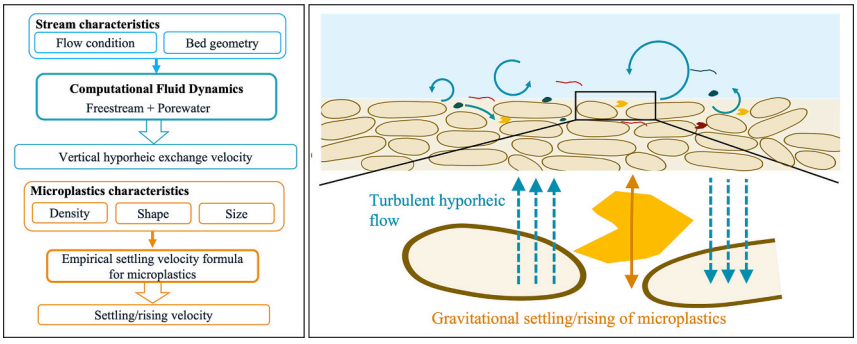

ARTICLE INFO

Editor: Kevin V. Thomas

Keywords:
Plastic pollution
Sediment-water interaction
Turbulent flow
Hyporheic exchange
Computational fluid dynamics (CFD)

ABSTRACT

Quantifying the impact of hyporheic exchange is crucial for understanding the transport and fate of microplastics in streams. In this study, we conducted several Computational Fluid Dynamics (CFD) simulations to investigate near-bed turbulence and analyze vertical hyporheic exchange. Different arranged spheres were used to represent rough and permeable sediment beds in natural rivers. The velocities associated with vertical hyporheic flux and the gravitational force were compared to quantify the susceptibility of microplastics to hyporheic exchange. Four scenario cases representing different channel characteristics were studied and their effects on microplastics movements through hyporheic exchange were quantitatively studied. Results show that hyporheic exchange flow can significantly influence the fate and transport of microplastics of small and light-weighted microplastics. Under certain conditions, hyporheic exchange flow can dominate the behavior of microplastics with sizes up to around 800 μm. This dominance is particularly evident near the sediment-water interface, especially at the top layer of sediments. Higher bed porosity enhances the exchange of microplastics between water and sediment, while increased flow conditions extend the vertical exchange zone into deeper layers of the bed. Changes in the bedform lead to the most pronounced vertical hyporheic exchange, emphasizing the control of morphological features on microplastics transport. Furthermore, it is found that sweep-ejection events are prevailing near the bed surface, serving as a mechanism for microplastics transport in rivers. As moving from the water column to deeper layers in the sediment bed, there's a shift from sweeps dominance to ejections dominance, indicating changes of direction in microplastics movement at different locations.

* Corresponding author.
E-mail address: hosein@vt.edu (H. Foroutan).

https://doi.org/10.1016/j.scitotenv.2023.167173
Received 7 August 2023; Received in revised form 6 September 2023; Accepted 15 September 2023
Available online 18 September 2023

1. Introduction

Microplastics (MPs), defined as plastic particles with various shapes and ranging in size from 1 μm to 5 mm, pose a significant environmental threat globally (Frias and Nash, 2019). Their presence in the aquatic ecosystems has been extensively documented (Cole et al., 2011; De Lucia et al., 2014; Enders et al., 2015; Qiu et al., 2015). MPs are persistent once enter the environment since finer particles are extremely difficult to remove, while larger plastic fragments continuously break down into smaller ones (Eerkes-Medrano et al., 2015; Rodríguez-Narvaez et al., 2021). Given the ubiquity, substantial magnitude, and inherent difficulty of addressing plastic pollution, it has now become a major topic in the environmental pollution research. While there are a wealth of studies focusing on MPs in the marine environment (Cole et al., 2011; De Lucia et al., 2014; Enders et al., 2015; Qiu et al., 2015; Ng and Obbard, 2006; Schmidt et al., 2018), surface water is often viewed only as a pathway for transporting plastic particles into the oceans (Schmidt et al., 2017; Van Wijnen et al., 2019; Akdogan and Guven, 2019). However, several studies have found abundant accumulation of MPs in river sediments, suggesting that river and streams are also a potential sink (Wagner et al., 2014; Peng et al., 2018; Li et al., 2018; Li et al., 2020; Adomat and Grischek, 2021). The accumulation of MPs in rivers leads to various issues as they leach toxic chemicals and may act as transport media for other harmful pollutants (Wagner et al., 2014; Issac and Kandasubramanian, 2021; Luo et al., 2019; Lambert and Wagner, 2018). Moreover, they can be easily consumed by microorganisms and wildlife. Due to their small size and non-biodegradability, the consumption of MPs can not only harm these microorganisms and wildlife, but also reach human through the food web (Castro et al., 2022; Cverenkárová et al., 2021; Lu et al., 2019). While there is limited knowledge about the impacts that these particles may have on living organisms, it is believed that MPs have the potential to negatively impact human health (Rodríguez-Narvaez et al., 2021; Lu et al., 2019; Fan et al., 2022). Given that humans are in close proximity to and have significant dependence on freshwater systems, it is crucial to pay more attention to microplastics in rivers.

Understanding the transport and fate of MPs in rivers are crucial in order to develop a mitigation strategy for plastic pollution in freshwater ecosystems. Nevertheless, despite the increasing interest in this topic, there remains a scarcity of research in this area. In a literature review conducted by Akdogan and Guven (2019), it was found that >50 % of the reviewed studies focused on MPs in the ocean, while only 11 % focused on MPs in rivers, with most of them primarily investigating occurrence and characterization rather than transport and fate. Additionally, when investigating the transport and fate of microplastics, research studies mostly place emphasis on the physical properties of MPs such as density and shape, or processes such as aging and biofouling that potentially influence these properties (Geissen et al., 2015; Horton and Dixon, 2018). These physical properties solely link the fate and transport of MPs to the gravitational force. However, it has been observed that buoyant MPs are present in river sediments, leading researchers to realize that gravitational force alone is insufficient to determine the fate of MPs, and the hyporheic exchange is another crucial factor in determining the fate of MPs in natural rivers (Frei et al., 2019; Lewandowski et al., 2019; Drummond et al., 2020; Yang et al., 2021).

Hyporheic exchange is a process of a bidirectional exchange of water, solute, and particles between the sediment bed and overlying water. It is driven by pressure variations and turbulence over the sediment-water interface (Boano et al., 2014; Grant et al., 2018a). Previous studies concerning the effect of stream flow on MP transport either used parameterized mass balance (Nizzetto et al., 2016), or only considered advective transport (Besseling et al., 2017), or quantified hyporheic exchange using solute tracer experiments (Drummond et al., 2020; Drummond et al., 2022). However, these methods do not explicitly account for the effect of turbulence that has been shown to potentially play a significant role in the hyporheic zone (Grant et al., 2018b). Consequently, it becomes challenging to fully comprehend the processes of MPs transport in the absence of detailed information on the fluid dynamics near the bed surface. Thus, accurately quantifying the impact of hyporheic exchange on the transport and fate of MPs at the sediment-water interface (SWI) requires approaches that represent turbulence with high fidelity.

To fill this research gap, Computational Fluid Dynamics (CFD) modeling is used in this study to provide detailed information on the turbulence near bed and to quantify the impact of hyporheic exchange on the transport and fate of MPs in rivers. CFD is particularly suitable for simulating three-dimensional turbulent flows near rough and permeable sediment beds. It enables the capturing of flow characteristics at the scale of sediment grains, thereby providing valuable insights into the impact of turbulence on the movement of MPs (Shen et al., 2022).

The aim of this study is twofold: firstly, to utilize CFD simulations to validate the importance of accounting for hyporheic exchange when investigating MPs transport and fate in rivers; and secondly, to leverage the detailed near-bed flow behavior obtained from CFD simulations to characterize the specific effects of different channel characteristics on the transport of MPs. The findings obtained from this study will contribute to a better understanding of the fate and transport of MPs in rivers.

2. Methods

In this study, we quantified the force exerted on microplastic particles by hyporheic exchange flow (HEF) and compared it to the gravitational force. To do that, we used a CFD model to calculate the vertical flow velocities in the water column and in the bed and used settling velocity formula to calculate the settling and rising velocity of microplastics particles. We then compared these two velocities to see which one is the dominant process responsible for the transport of MPs at the sediment-water interface. Moreover, we quantified the correlation between the velocity fluctuations in streamwise and vertical directions to investigate the effect of near-bed turbulence on motions of MPs.

2.1. Vertical hyporheic exchange rate

Hyporheic flow moves along the streamwise, spanwise and vertical directions. Here, we focus on the vertical exchange that alters the behavior of MPs under the gravitational force. The vertical hyporheic exchange rate is represented by the vertical velocity of the flow.

2.1.1. Turbulence modeling

The CFD simulation involves numerically solving the transport equations of mass and momentum within a defined computational domain, while taking into account the specified initial and boundary conditions. It is crucial to consider the impact of fluctuating turbulent motions within the flow, as they play a significant role in the mass and momentum transport, necessitating their inclusion in the simulation.

We employed the Detached Eddy Simulation (DES) modeling approach to accurately capture the turbulent flow both near and inside the bed. The DES model, initially introduced by Spalart et al., is based on the one-equation Spalart-Allmaras Reynold-Averaged Navier-Stokes (RANS) model (Spalart et al., 1997). It combines the advantages of Large Eddy Simulation (LES) models, allowing for the resolution of time-dependent, three-dimensional turbulent structures. By providing detailed information on velocity fluctuations near the sediment-water interface, it enhances our understanding of flow behavior and its potential impact on fine particles (Rodi, 2010). Moreover, DES significantly reduces the computational cost associated with LES by employing unsteady RANS. This approach is particularly beneficial in the boundary layer, where LES is constrained by computational grid resolution. Specifically, the delayed DES (DDES) model was used in this study, which is an improved version of the original Spalart-Allmaras DES model. The original DES model has been shown to encounter problems where the

computational grid is locally refined since the transition from LES to RANS is determined by comparing the RANS length scale to the maximum grid cell length. When the grid is locally refined, the eddy viscosity in the boundary layer can be decreased too much to transfer modeled turbulence energy into resolved energy. In our study, since we have highly curved geometries, i.e., sediment gravels, local grid refinements are unavoidable. By using DDES, this issue can be addressed since the model incorporates a flow dependent shielding function that prevents the switch from RANS to LES mode within the attached boundary layers (Spalart et al., 2006). The governing equations for the DDES model are presented in the supplementary document.

The present modeling framework was validated against the measurements obtained in the lab experiments done by Manes et al. and the LES modeling results by Lian et al. (Manes et al., 2009; Lian et al., 2019) The validation was performed by comparing the double-averaged streamwise velocity components as described in Section 2.1.4. The comparison (see Fig. S1 in the supplementary document) shows that our DDES model gives good results, especially near the SWI. The close agreement with previous measurements and modeling results gives us confidence in investigating hyporheic flow behavior with our modeling framework.

2.1.2. Computational setup

The computational domain encompassing the water and sediment bed had dimensions of 1.1 m × 0.55 m × 0.45 m, carefully selected to prevent spanwise locking and allow for the avoidance of significant turbulent structure interactions. The permeable flat sediment bed is represented by body-centered cubic packing monodisperse spheres. The mounded bedform is generated with randomly arranged polydisperse spheres to mimic a more realistic bedform. The configuration of the computational domain ensures a comprehensive simulation of the water column and permeable sediment bed as an integrated system. This approach eliminates the need for additional parameterization or coupling, enabling accurate representation of water movement both within and outside the bed. As a result, we obtain reliable information regarding hyporheic exchange flow. The entire computational domain was discretized by an unstructured curvilinear mesh that fit to the watertight geometry representing the permeable riverbed. The total number of grids varied between 31,411,047 and 33,494,942, depending on the specific case scenario. The mesh is refined around the bed so that the model can resolve interfacial turbulent structures between gravels. The smallest grid sizes of 0.8 mm were used in the bed region and at the sediment-water interface. Moving towards the freestream, the grid sizes gradually increase, reaching a size of 2.5 mm. The grid size in the wall units, calculated as $\Delta z^+ = u_* \Delta z/\nu$, ranges from 14.4 to 45, which is comparable to those used in a similar previous study (Han et al., 2019).

The unsteady DDES simulations were initialized using converged results from Spalart-Allmaras RANS simulation. In these RANS simulations, cyclic boundary conditions were employed at the side boundaries to represent an extended domain in the spanwise direction since we were only simulating a small region in the middle of the river. The upper and lower patches were set as slip boundaries (zero normal velocity and zero normal gradients of all other variables), assuming an undisturbed free surface and a deep Darcy flow within the sediment bed. For the inlet boundary condition, we defined a fixed turbulent velocity profile artificially generated to achieve the desired bulk Reynolds number. The outlet boundary condition was set to a zero gradient. The precursor RANS model was then iterated until convergence, and its output results for the velocity and turbulence levels within the domain were used as the initial conditions for the DDES simulations. Prior to commencing the DDES simulations, the boundary conditions at the inlet and outlet were changed to periodic, mimicking an infinitely long river. Additionally, a body force was applied to the momentum equation to drive the flow. A similar approach has been used by Moin and Kim, and Lian et al. (Lian et al., 2019; Moin and Kim, 1982)

2.1.3. Test case scenarios

Four case scenarios were considered in this study. In the base case scenario, a bed with a thickness of 0.15 m and a porosity of 0.4 was constructed using spheres with a diameter of 25 mm (D = 25 mm). The chosen values of porosity and gravel size are associated with uniform gravel beds in natural streams and fall within the range used by previous studies (Brosten et al., 2009; Wang et al., 2021; Ling et al., 2022; Zhou and Endreny, 2013; Kazezyılmaz-Alhan and Medina, 2006). The free-stream depth H was 0.3 m. The approach flow velocity U was 0.18 m/s resulting in the Reynolds number for the bulk flow ($Re = UH/\nu$) to be 54,000. The second case was the high flow scenario, where we doubled the bulk Reynolds number by setting the approach flow velocity to be 0.36 m/s, while keeping other parameters the same as the base case. The Froude number of the two flow conditions are 0.1 and 0.21, which are both smaller than 1, so the assumption of undisturbed free surface was applicable. The purpose of the third case was to investigate the impact of porosity. In this case, we modified the bed porosity to 0.45, aiming to simulate a bed with higher permeability. In the fourth case, a mounded bedform was introduced onto the surface of the flat bed. A mound with a height of 70 mm was positioned at the center of the bed. To maintain consistency, the porosity of the mound was set to be the same as that of the bed. Detailed information regarding the four cases can be found in Table 1.

2.1.4. Simulations and post-processing

The open-source finite-volume CFD package OpenFOAM v9 was used for the simulations. The code was fully parallelized and ran using 128 processors on a high-performance computing system at Virginia Tech. All simulations were conducted for 20 flow-through times (the time required by the mean flow to pass through the domain once) to ensure that the flow is fully turbulent, and then the velocities were time-averaged over another 20 flow-through times. To better understand the patterns in the velocity profiles, the time-averaged velocities were averaged over a specific volume to obtain double-averaged velocities using Eq. (1) (Lian et al., 2021).

$$< \overline{u_i} >= \frac{1}{V_F}\int_{V_F} \overline{u_i} dV \tag{1}$$

where $\overline{u_i}$ is the time-averaged velocity V_F is the fluid volume within the averaging volume V. In this study, the averaging volume V extends across the domain in both the x and y directions and has a thickness of 5 mm in the z direction. The chosen thickness of 5 mm aligns with the definition of microplastics, which refers to plastic particles with sizes smaller than 5 mm.

2.2. Settling and rising velocities

The settling and rising velocities of microplastics were calculated using the formulation developed by Waldschläger and Schüttrumpf that considers the density, shape, and size of microplastic particles (Waldschläger and Schüttrumpf, 2019).

$$w_x = \sqrt{\frac{4}{3}\frac{d_{eq}}{C_D}\left|\frac{\rho_s - \rho}{\rho}\right| g} \tag{2}$$

In Eq. (1), ρ_s and ρ are microplastics and water densities, respectively. The settling and rising velocities for various shapes of microplastic particles are derived by using different formulations for the drag coefficient C_D and the equivalent diameter d_{eq}.

The drag coefficient for the settling velocities is:

$$C_D = \begin{cases} \dfrac{3}{CSF \times \sqrt[3]{Re}} & \textit{pellet and fragments} \\ \dfrac{4.7}{\sqrt{Re}} + \sqrt{CSF} & \textit{fiber} \end{cases} \tag{3}$$

Table 1
Scenarios and the corresponding river channel properties. The simulated river flow is directed along the x-axis.

Case	Base	High flow	Large porosity	Mounded bed
Domain	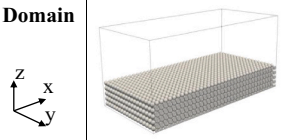	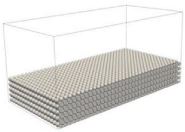	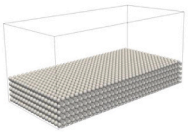	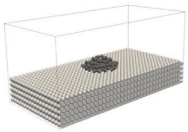
Stream wise velocity	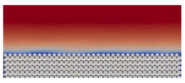	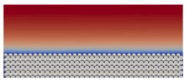	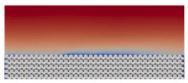	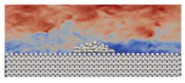
Porosity	0.4	0.4	0.45	0.4
Bulk velocity	0.18 m/s	0.36 m/s	0.18 m/s	0.18 m/s

And that for the rising velocities is:

$$C_D = \begin{cases} \left(\frac{20}{Re} + \frac{10}{\sqrt{Re}} + \sqrt{1.195 - CSF}\right) \times \left(\frac{6}{P}\right)^{1-CSF} & pellet\ and\ fragments \\ \frac{10}{\sqrt{Re}} + \sqrt{CSF} & fiber \end{cases} \tag{4}$$

Here, P is the powers roundness, and CSF is the Corey Shape Factor of particles, calculated with shortest side length a, intermediate side length b, and longest side length c:

$$CSF = \frac{c}{\sqrt{ab}} \tag{5}$$

Re is the particle Reynolds number, calculated using kinematic viscosity ν and the particle velocity w_x:

$$Re = \frac{w_x d_{eq}}{\nu} \tag{6}$$

The equivalent particle diameter is defined as:

$$d_{eq} = \begin{cases} \sqrt[3]{abc} & pellet\ and\ fragments \\ c & fiber \end{cases} \tag{7}$$

This formula was shown to be more accurate than using the Stokes law (Waldschläger and Schüttrumpf, 2019), which was used by a number of previous studies concerning microplastics fate and transport in streams (Drummond et al., 2020; Besseling et al., 2017). By incorporating the Reynolds number of particles, it accounts for the small-scale turbulent motions that arise during particle settling or rising.

3. Results and discussion

In this section, we undertake a comprehensive study to investigate the influence of river characteristics on the turbulent flow over and within the permeable bed, and its consequential effect on the fate and transport of microplastics. To accomplish this, we analyze the model output in three distinct stages. Initially, the profiles of double-averaged vertical component of flow velocity are presented. This is followed by quadrant analysis, an established method to investigate the near-bed turbulence, in the near-bed water column, at the sediment-water interface, and in the transition layer (Wallace, 2016). Finally, we compared the vertical flow velocities and microplastics settling and rising velocities.

3.1. Vertical velocity profiles

For all four test cases described above, the vertical velocities were plotted in Fig. 1 against normalized elevation, denoted as z*. In this representation, the sediment water interface is at z* = 0, values below 0 correspond to the bed, and values above 0 represent the overlying water. All velocities were double averaged over time and volume as described in the method. For all cases except for the mounded bed case, the averaging volume was expanded over the whole domain in the streamwise and spanwise direction. For the bedform case, before the volume averaging, the entire domain was divided into five sections (see Fig. S3): in front of the mound, at the windward side of the mound, at the middle of the mound, at the leeward side of the mound, and behind the mound. This division was done to closely examine the flow behavior at and in the vicinity of the mound.

In the base case, the bulk Reynolds number was 54,000, and the water was flowing freely over and through a flat permeable bed. Negative vertical velocities are observed above the SWI (Fig. 1a). This indicates the dominance of downwelling flow in the shear layer, albeit not very intense. Notably, the vertical flow velocity peak at the first layer of spheres, reaching high velocities of up to 1 mm/s. This observation suggests intense vertical hyporheic exchange in this region.

In the high flow case, where the bulk flow velocity was doubled, so as the bulk Reynolds number, the maximum upwelling velocity remain unchanged, while the downwelling velocity significantly increases from nearly 0 to 0.5 mm/s (Fig. 1a). Furthermore, the high vertical velocity extends deeper into the bed, expanding the region of intense hyporheic exchange vertically. These findings suggest that under high flow conditions, the flow may push more MPs further into the bed and mobilize those situated deeper in the sediment column.

In the case of a large porosity bed, with the same bulk flow velocity as the base case, the high vertical velocity region contracts back to the first layer of bed. However, as shown in Fig. 1b, the maximum velocity slightly increases to approximately 1.1 mm/s, indicating a slight increase in the propensity for the transport of MPs.

In the case of a mounded bedform, notable and substantial alterations in flow behavior are observed both within the bed and throughout the water column. Fig. 1c shows that in front of the mound, the maximum vertical velocity in the bed has the same magnitude as that in the base case, but the high velocity region is extended to almost the bottom of the study domain, pushing MPs even deeper than the high flow condition. The turbulence induced by the bedform also disturbed the water column, increased the downwelling flow velocity compared to other cases. As a consequence of this increase, it is likely that certain floating MPs will be pushed downward and eventually settle on the bed. In the back of the mound, the HEF has high upwelling velocity,

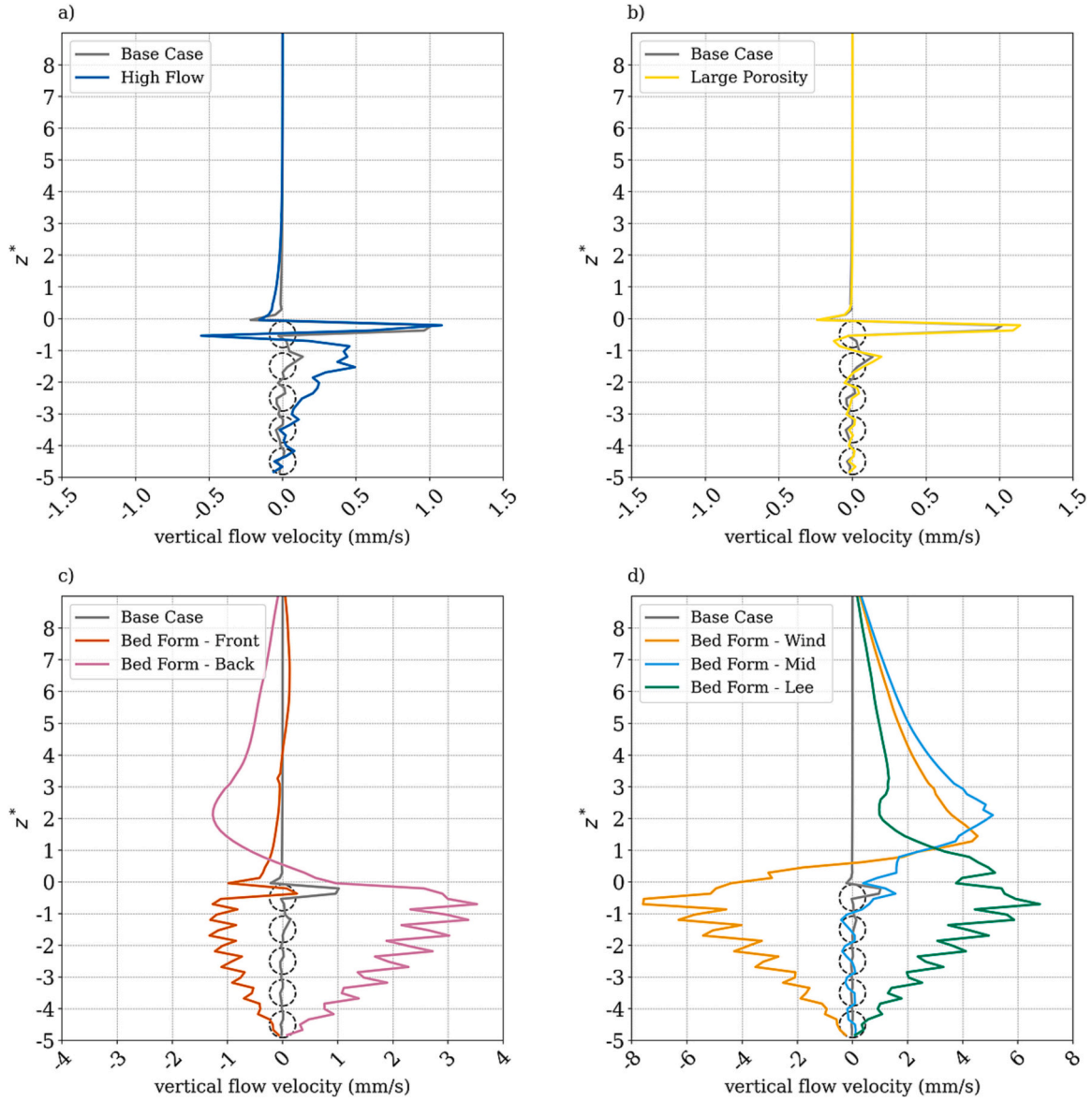

Fig. 1. Comparisons of double-averaged vertical velocity profiles between the base case and high flow case (a), large porosity case (b), and mounded bedform case (c and d). The elevation z is normalized by one cubic packed sphere unit (0.03 m). The spheres plotted with dashed lines represents the sphere layers in the sediment bed.

mobilizing and transporting MPs out of the bed. Furthermore, the transition from downwelling to upwelling velocity in the water column suggests the presence of a recirculation zone, which could potentially have an impact on the transport of MPs.

The pumping effect shown in the vicinity of the mound is even more prominent at the mound. The range of vertical flow velocity is >10 times larger than all other cases as shown in Fig. 1d. The downwelling vertical HEF has the velocity up to approximately 8 mm/s, while the high velocity region is also extended to the bottom of the study domain. In the middle portion of the mound, the magnitude of velocity decreases to the level of the base case below the original bed elevation. However, within the mound itself ($0 < z^* < 2.5$), the upwelling velocity becomes dominant. As to the leeward side, the upwelling hyporheic velocity becomes even larger indicating that the MPs pushed inside the mound from the windward side may get flushed out. Additionally, there is high upwelling velocity in the water column above the mounded bed in spite of location, which may indicate that at least a range of MPs are kept from getting into the mounded bed by the flow.

Based on the vertical flow velocity profiles, it is evident that in a permeable sediment bed, the most significant hyporheic exchange occurs within the top layer of sediment particles. This finding aligns with previous studies indicating that the Brinkman layer thickness is on the order of the particle diameter (Goharzadeh et al., 2005; Goharzadeh et al., 2006). Moreover, the results show that under high flow conditions or when bedform changes occur, there is a consistent presence of relatively high vertical velocity in the deeper layers of sediment. This observation suggests that a potentially significant vertical exchange of solute or particles still exists within the Darcy layer.

3.2. Flow behavior near the sediment-water interface

The quadrant analysis of the instantaneous velocity fields is adopted to gain further insight into the HEF near the sediment-water interface. To accomplish this, we presented the turbulent fluctuations in four quadrants with respect to the vertical and streamwise directions. The events in the four quadrants are called outward interactions ($u' > 0, w' > 0$), ejections ($u' < 0, w' > 0$), inward interactions ($u' < 0, w' < 0$), and sweeps ($u' > 0, w' < 0$), respectively (Wallace et al., 1972). Among these

four types of bursting events, sweeps and ejections occur more frequently, particularly in the vicinity of and at the sediment-water interface (Cooper et al., 2018). The occurrence of sweep-ejection events contributes to the transport of momentum, solutes, and sediments, thereby influencing particle entrainment and displacement, as well as altering concentration profiles (Han et al., 2018; Bernard and Handler, 1990; Cameron et al., 2020; Tsai and Huang, 2019).

The quadrant analysis of the four cases at different locations (Fig. S4) are presented in Fig. S5, where the size of bubbles represents the magnitude of production of turbulence fluctuations, the color represents the magnitude of the uw component of Reynolds shear stress (RSS). The values of u', w', and RSS are normalized by the friction velocity u*. u* can be calculated as $(\tau_w/\rho)^{0.5}$, where $\tau_w = hdp/dx$ (Lian et al., 2019; Han et al., 2019). In this study, the pressure gradient dp/dx that drives the flow is the body force term added in the momentum equation. The joint probabilities of the four bursting events are plotted in Fig. 2.

In the water column, the results (Fig. S5.1 & Fig. 2) show that sweep-ejection events dominate near the wall, occurring with a frequency exceeding 80 %. Sweeps contribute slightly more than ejections, except for the high flow case. Hence, high flow conditions may reduce the likelihood of MPs near the bed surface being entrained into the bed.

At the SWI, the sweep phenomenon becomes more prominent in the base case and high flow case, indicating the enhanced vertical transport of MPs towards the bed. This aligns with the finding we got from the velocity profiles. In all cases except for the mounded bedform case, sweep events contribute more than ejections. The difference between sweeps and ejections corroborates the finding in previous studies that sweeps dominate near the bed surface (Shahiri Tabarestani et al., 2021; Mangan et al., 2022). It should be noted that the pie chart for the bedform case may be slightly inaccurate because the distinction in the occurrence of sweeps and ejections may be compromised due to the canceling effect of the quasi-steady downward velocity in front of the mound and the upward velocity behind the mound.

Within the transition layer, there is a significant increase in the

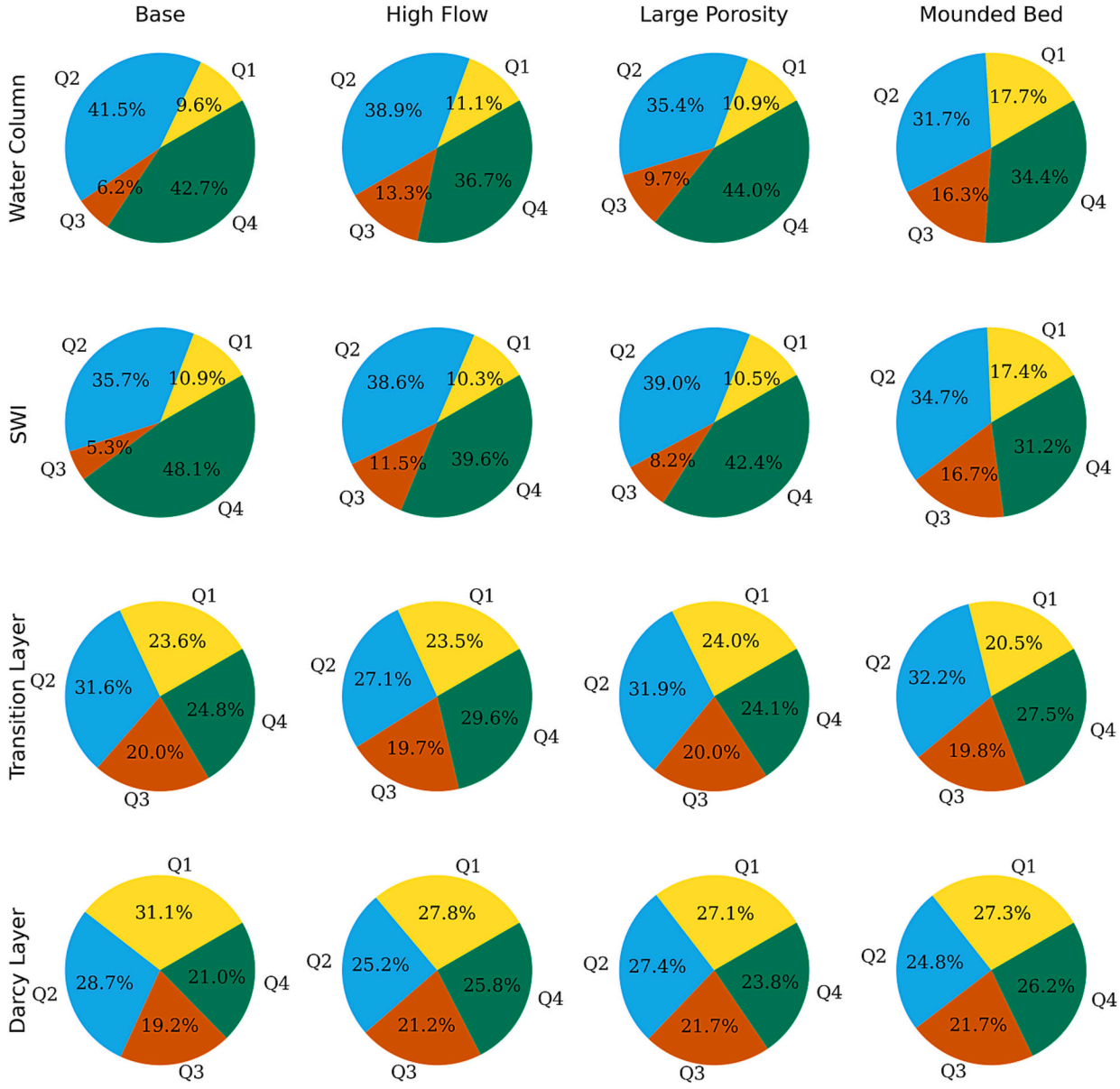

Fig. 2. Plots of the bursting events probability for Base case (column 1), High flow case (column 2), Large porosity case (column 3), and Mounded bedform case (column 4). The top row shows the analysis at the representative *xy* plane of water column (z* = 0.5). The second row shows the analysis at the sediment-water interface (SWI; z* = 0). The third row shows the analysis at the representative *xy* plane in the transition layer (z* = −0.5). The bottom row shows the analysis at the representative *xy* plane of the Darcy layer (z* = −1.5). Locations of these four planes are presented in Fig. S4 in the supplementary document.

magnitudes of turbulence fluctuation production compared to other layers, as shown in Fig. S5. This may be due to the turbulence that penetrates, and the vortices induced by, the top layers of sediments. Interestingly, the occurrence of the four quadrant events appears to be similar (Fig. 2), suggesting a gradual shift from turbulent flow to Darcy flow regime. Fig. S5.3 shows that the magnitudes of turbulence fluctuation production are larger in Q2 and Q4 compared to Q1 and Q3, which may result from the presence of interstitial vortices, illustrating that the sweeps and ejections remain highly efficient in the transport of MPs within the transition layer. Additionally, it should be noted that in quadrant 4, intense Reynolds shear stress occurs along with a long tail in the streamwise direction, indicating vertical motions towards the deep bed and horizontal motion downstream.

In the Darcy layer (Fig. S5.4), the magnitudes of dimensionless RSS decrease significantly compared to other locations, to an average magnitude of about 0.1. The probability of ejection-sweep events becomes comparable to that of inward-outward interactions. However, the magnitude of velocity fluctuation production in quadrant 4 is still quite large, similar to that at the SWI. This may result in descending motion of MPs in the Darcy layer.

By comparing the bubble plots in Fig. S5, we observe that the shapes of the bubble clouds are similar at different locations across the four cases. However, it is important to note that in the mounded bedform case, the reference size of bubbles is 2 to 4 times larger than in the other cases. This indicates more intense vertical motions of MPs. Furthermore, we can observe that the bubble cloud expands along the vertical axis and contracts along the horizontal axis as we move from the water column to deeper layers within the sediment bed. This trend suggests that vertical motions gradually become more dominant compared to streamwise displacement motions. Consequently, once MPs descend beyond a certain depth, they may tend to remain there rather than being transported downstream.

3.3. Hyporheic and settling/rising velocity comparisons

Microplastic particles possess intrinsic properties such as density, shape, size, and roundness, which dictate their behavior in still water due to gravitational forces. Our objective is to understand how and when hyporheic exchange flow alter the behavior of microplastics, and subsequently influence their fate and transport in streams. To achieve this goal, we compared and balanced the upward (downward) hyporheic velocity with the settling (rising) velocity of microplastics. In this comparison, we considered the following polymer types: Polyethylene (PE), Polypropylene (PP), Polystyrene/Expanded Polystyrene (PS/EPS), Polyvinyl Chloride (PVC), Polyethylene Terephthalate (PET), and Copolyamide (CoPA). For PVC, PS, and EPS, we considered the shapes of spheres, pellets, and fragments. For PET, PP, and PE, we included the shapes of spheres, pellets, fragments, and fibers. However, for CoPA, we only focused on the fiber shape. These combinations of types and shapes of MPs were chosen because they are commonly found and studied in surface waters and sediments (Wang et al., 2017; Osorio et al., 2021). Furthermore, their inclusion in a previous study where settling and rising velocities of microplastics were determined ensures the accuracy of the calculated velocities. The density and shape of these MPs were kept consistent with the study conducted by Waldschläger and Schüttrumpf (2019), while for particle sizes, we expanded the range to cover the entire size range defined for microplastics, ranging from 1 μm to 5000 μm. We then obtained a threshold size that determines the shift from hyporheic exchange dominance to gravity dominance, so MPs with sizes smaller than the threshold would be primarily influenced by the HEF.

Fig. 3 presents the ratio of the maximum hyporheic velocity to the settling or rising velocity of various types and shapes of MPs plotted against the size of microplastic particles. The ratios are categorized based on the combination of polymer type and shape, and they are represented as shaded areas in the plots for each classification. The horizontal lines indicate the point at which the settling or rising velocity equals the maximum hyporheic exchange velocity. When the plotted shades lie above these lines, it indicates that the behavior of MPs with corresponding sizes is predominantly influenced by hyporheic flow. The values of threshold sizes are presented in Table 2.

As shown in Fig. 2a, the maximum upward hyporheic velocity in the base case, high flow case, and large porosity case are comparable. In contrast, in the mounded bed case, the maximum velocity is approximately seven times larger compared to the other cases, consistent with the findings from the velocity profiles section. Among the four types of microplastics studied, PS pellets and fragments exhibit the highest susceptibility to hyporheic exchange, with a threshold size of 460 μm for the mounded bedform case and around 70 μm for other cases, which are approximately twenty times larger than those of PET, PVC, and CoPA. CoPA fibers are the second most susceptible, with a threshold size of 100 μm for the mounded bedform case and approximately 25 μm for the other three cases. In contrast, the impact of hyporheic exchange on PVC pellets and PET pellets and fibers is negligible in the base case, high flow case, and large porosity case, as the flow only affects particles with sizes smaller than 5 μm for pellets and 10 μm for fibers. Based on the results, it is evident that for MPs with a density higher than that of water, the threshold size increases as the density difference from water decreases. Consequently, a larger threshold size implies that a greater number of microplastics will be influenced by hyporheic flow. Additionally, when MPs have the same density, it is observed that fibers are more susceptible to the effects of hyporheic flow.

In the comparison between the maximum downward hyporheic velocity and the rising velocity (Fig. 2b), it is noteworthy that most threshold sizes are larger than those observed in the settling velocity comparisons. This difference arises due to the fact that buoyant microplastics generally exhibit smaller density variations with water when compared to settling microplastics. In this comparison, the base and the large porosity cases yield similar results. Under high flow conditions, the threshold sizes for all types of microplastics are approximately two times larger than in the base case. In the mounded bedform case, the threshold sizes are around 10 times larger for pellets and fragments and around 40 times larger for fibers compared to the base case. Interestingly, buoyant pellets and fragments are more susceptible than fibers, with threshold sizes ranging from 2 to 10 times larger depending on different stream characteristics, such as the bulk flow velocity, porosity, and the bedform.

The velocity comparisons reveal that MPs with smaller sizes and smaller density differences from water are more susceptible to the hyporheic flow. Interestingly, we notice a contrasting pattern in the influence of microplastic shapes on their behavior. For buoyant microplastics, those with spherical, pellet, and fragment shapes exhibit a higher susceptibility to hyporheic flow, while for sinking microplastics, the dominance of flow is more pronounced for fiber shape. The threshold sizes in Table 2 show that under same stream characteristics, buoyant MPs are generally more prone to hyporheic flow than non-buoyant MPs. The flow can transport buoyant MPs towards the sediment bed (Molazadeh et al., 2023), which explains the presence of lightweight MPs in sediment. These comparisons provide validation for the influence of hyporheic flow on the behavior of MPs. As hyporheic flow exerts forces on MPs that are either opposing or in the same direction as gravitational forces, it undoubtedly affects the residence time of MPs in rivers, as highlighted in a previous study (Drummond et al., 2022).

4. Conclusion

This study investigated the influence of near-bed turbulence on the fate and transport of MPs in river systems. By comparing velocities resulting from the gravitational force and the hyporheic exchange, we demonstrated that MPs may be influenced by hyporheic exchange flow in streams, with smaller and buoyant microplastics exhibiting higher susceptibility. Additionally, particles with the shape of sphere,

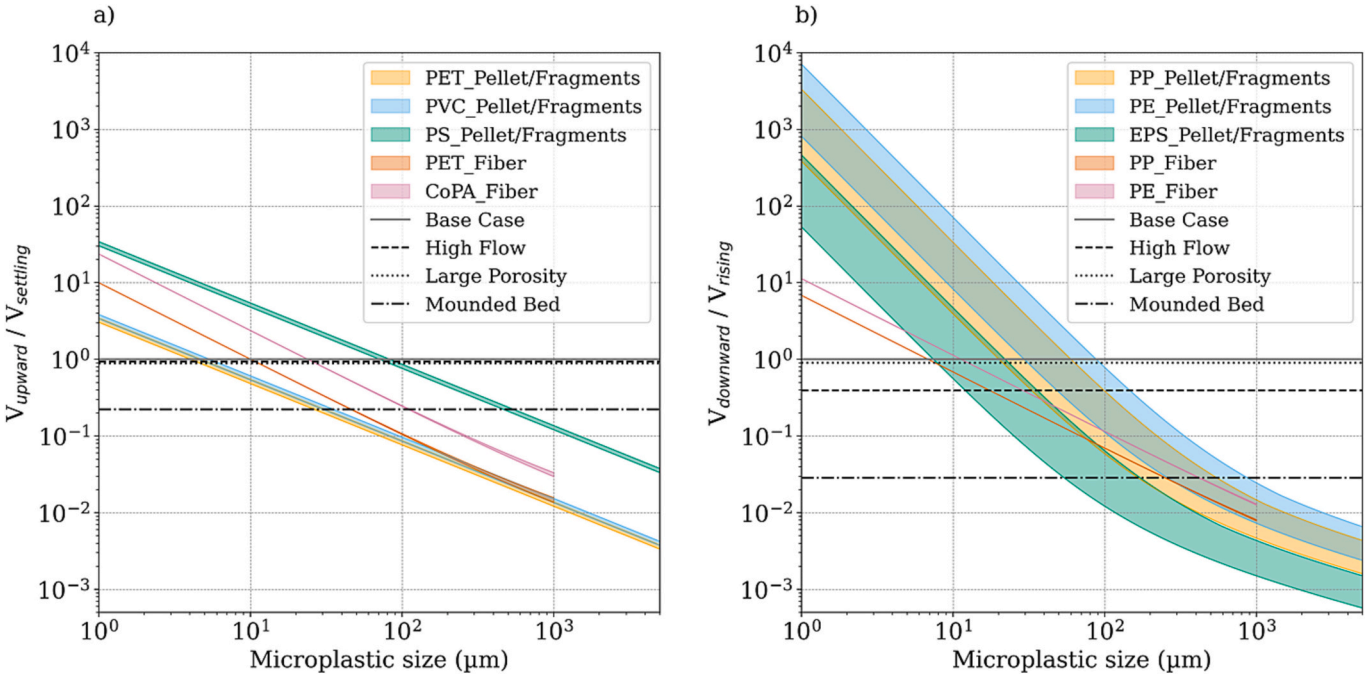

Fig. 3. Ratio of upward hyporheic exchange velocity to settling velocity (a), and downward hyporheic exchange velocity to rising velocity (b). The ratios are plotted against the MP size (chosen as the longest side length c) for all microplastic combinations of different size, shape (defined by CSF and P), and density, and are classified by density (polymer type) and shape (fiber or pellet/fragment). The horizontal lines indicate $V_{vertical\ flow} = V_{settling/rising}$ for four cases.

Table 2
The maximum sizes of settling (a) and floating/rising (b) microplastic particles influenced by upward and downward flow, respectively. All sizes are in the unit of µm.

(a)	PET (Spheres, Pellet, Fragments)	PVC (Spheres, Pellet, Fragments)	PS (Spheres, Pellet, Fragments)	PET (Fiber)	CoPA (Fiber)
Base	4	4	71	10	23
High Flow	4	4	76	10	25
Large Porosity	4	5	82	11	26
Mounded Bed	26	29	460	45	108

(b)	PP (Spheres, Pellet, Fragments)	PE (Spheres, Pellet, Fragments)	EPS (Spheres, Pellet, Fragments)	PP (Fiber)	PE (Fiber)
Base	60	88	22	6	11
High Flow	99	146	36	17	29
Large Porosity	63	93	23	7	12
Mounded Bed	548	874	171	252	423

fragment, or pellet, were found to be more prone to hyporheic exchange flow among buoyant MPs, whereas fibers showed higher susceptibility among non-buoyant MPs. The analysis of four different cases with varying channel characteristics revealed distinct flow behaviors and hyporheic exchange patterns, providing valuable insights into the impact of hyporheic exchange on MPs entrainment and deposition. In the base case featuring a flat permeable bed, a downwelling flow near the SWI was observed, along with significant vertical exchange in the top sediment layer, suggesting enhanced transport of MPs at this location. Increasing the bulk flow velocity expands the region of vertical hyporheic exchange, indicating that high flow conditions can intensify the vertical motion of MPs. Comparison between different bed porosity cases showed that a more permeable bed facilitates the transport of MPs. Importantly, changes in bed morphology exhibited the most pronounced influence on flow behavior, highlighting the dominant control of morphological features on vertical hyporheic exchange and subsequent microplastic transport. The quadrant analysis of bursting events revealed the prevalence of sweep-ejection events near the sediment-water interface, which plays a crucial role in facilitating the transport of MPs. Despite variations in intensity, the patterns of the occurrence of bursting events provided valuable information for predicting the motion of MPs at different depths near and within the sediment bed.

Although the results of this study provide valuable insights into the transport and fate of MPs in streams, there are certain limitations that should be acknowledged. Firstly, this study consisted solely of scenario tests focused on a limited number of specific combinations of river properties. Plus, the formulas for settling and rising velocities were obtained from a study using virgin MPs, while in the aquatic environment, weathering processes and aggregation and flocculation with sediments may impact these velocities (Waldschläger et al., 2020; Karkanorachaki et al., 2021; Serra and Colomer, 2023; Laursen et al., 2023), and hence, the findings only provide a partial understanding of the microplastic dynamics in real world rivers. Therefore, before applying these results to analyze the transport of MPs in real rivers, careful examination and consideration of their applicability are necessary. For example, the threshold sizes of MPs in Table 2 were calculated based on the specific settings of the scenario cases. Given the varying degrees of significance that different river properties can have on MPs' transport,

we recommend assessing the similarity of bedform conditions (flat or mounded) and flow conditions (bulk Reynolds number) before applying the values from the table to real-world channels. This precaution will ensure the appropriate application of the calculated values in practical situations. Moreover, future studies could broaden the scope of scenarios cases to include channels with irregular packed bedform and lower porosity to explore varying natural conditions related to hyporheic exchange and MPs transport. Additionally, the CFD models utilized in this study, while are validated with lab experiment data, used simplified regularly packed bed geometry and a relatively coarse mesh to reduce computational costs, which may potentially impact the generalizability of the results. Furthermore, it should be noted that the study focused on the impact of vertical hyporheic flow on MPs transport, and other particle-flow interaction processes were not considered. These limitations point to the need for further research in two areas: 1) To refine the modeling framework in terms of the geometry and computational setup and apply it to real test cases by incorporating field-measured data such as stream characteristics and MP concentrations; and 2) to model MP particles in river ecosystems with an Eulerian-Lagrangian framework to account for additional transport mechanisms (Molazadeh et al., 2023; Bigdeli et al., 2022; Summers et al., 2023).

Overall, the findings of this study contribute to our understanding of the dynamics of microplastic transport and fate in rivers, particularly through the influence of hyporheic exchange flow. Also, this study serves as a demonstration of the advantages offered by high-fidelity fluid dynamics simulations in microplastics research. Such simulations enable more effective and accurate results, allowing for the capture of small-scale motions near the bed that cannot be directly measured, and thereby, help filling the research gap regarding the transport and fate of MPs in streams.

Funding

This work is partially supported by the National Science Foundation (NSF) under Award Numbers 2039692 and 2145532.

CRediT authorship contribution statement

Huan Yang: Methodology, Software, Formal analysis, Validation, Visualization, Writing – original draft. **Hosein Foroutan:** Conceptualization, Investigation, Supervision, Funding acquisition, Writing – review & editing.

Declaration of competing interest

The authors declare that they have no known competing financial interests or personal relationships that could have appeared to influence the work reported in this paper.

Data availability

The data are available within figures and tables in the manuscript and supplementary document.

Appendix A. Supplementary data

Supplementary data to this article can be found online at https://doi.org/10.1016/j.scitotenv.2023.167173.

References

Adomat, Y., Grischek, T., 2021. Sampling and processing methods of microplastics in river sediments - a review. Sci. Total Environ. 758, 143691. https://doi.org/10.1016/j.scitotenv.2020.143691.

Akdogan, Z., Guven, B., 2019. Microplastics in the environment: a critical review of current understanding and identification of future research needs. Environ. Pollut. 254, 113011. https://doi.org/10.1016/j.envpol.2019.113011.

Bernard, P.S., Handler, R.A., 1990. Reynolds stress and the physics of turbulent momentum transport. J. Fluid Mech. 220, 99–124. https://doi.org/10.1017/S0022112090003202.

Besseling, E., Quik, J.T.K., Sun, M., Koelmans, A.A., 2017. Fate of nano- and microplastic in freshwater systems: a modeling study. Environ. Pollut. 220, 540–548. https://doi.org/10.1016/j.envpol.2016.10.001.

Bigdeli, M., Mohammadian, A., Pilechi, A., Taheri, M., 2022. Lagrangian modeling of marine microplastics fate and transport: the state of the science. J. Mar. Sci. Eng. 10 (4), 481. https://doi.org/10.3390/jmse10040481.

Boano, F., Harvey, J.W., Marion, A., Packman, A.I., Revelli, R., Ridolfi, L., Wörman, A., 2014. Hyporheic flow and transport processes: mechanisms, models, and biogeochemical implications: hyporheic flow and transport processes. Rev. Geophys. 52 (4), 603–679. https://doi.org/10.1002/2012RG000417.

Brosten, T.R., Bradford, J.H., McNamara, J.P., Gooseff, M.N., Zarnetske, J.P., Bowden, W.B., Johnston, M.E., 2009. Multi-offset GPR methods for hyporheic zone investigations. Surf. Geophys. 7 (4), 247–257. https://doi.org/10.3997/1873-0604.2008034.

Cameron, S.M., Nikora, V.I., Witz, M.J., 2020. Entrainment of sediment particles by very large-scale motions. J. Fluid Mech. 888, A7. https://doi.org/10.1017/jfm.2020.24.

Castro, G.B., Bernegossi, A.C., Pinheiro, F.R., Corbi, J.J., 2022. The silent harm of polyethylene microplastics: invertebrates growth inhibition as a warning of the microplastic pollution in continental waters. Limnologica 93, 125964. https://doi.org/10.1016/j.limno.2022.125964.

Cole, M., Lindeque, P., Halsband, C., Galloway, T.S., 2011. Microplastics as contaminants in the marine environment: a review. Mar. Pollut. Bull. 62 (12), 2588–2597. https://doi.org/10.1016/j.marpolbul.2011.09.025.

Cooper, J.R., Ockleford, A., Rice, S.P., Powell, D.M., 2018. Does the permeability of Gravel river beds affect near-bed hydrodynamics?: permeability of gravel river beds and near-bed hydrodynamics. Earth Surf. Process. Landf. 43 (5), 943–955. https://doi.org/10.1002/esp.4260.

Cverenkárová, K., Valachovičová, M., Mackuľak, T., Žemlička, L., Bírošová, L., 2021. Microplastics in the food chain. Life 11 (12), 1349. https://doi.org/10.3390/life11121349.

De Lucia, G.A., Caliani, I., Marra, S., Camedda, A., Coppa, S., Alcaro, L., Campani, T., Giannetti, M., Coppola, D., Cicero, A.M., Panti, C., Baini, M., Guerranti, C., Marsili, L., Massaro, G., Fossi, M.C., Matiddi, M., 2014. Amount and distribution of neustonic micro-plastic off the Western Sardinian coast (Central-Western Mediterranean Sea). Mar. Environ. Res. 100, 10–16. https://doi.org/10.1016/j.marenvres.2014.03.017.

Drummond, J.D., Nel, H.A., Packman, A.I., Krause, S., 2020. Significance of hyporheic exchange for predicting microplastic fate in rivers. Environ. Sci. Technol. Lett. 7 (10), 727–732. https://doi.org/10.1021/acs.estlett.0c00595.

Drummond, J.D., Schneidewind, U., Li, A., Hoellein, T.J., Krause, S., Packman, A.I., 2022. Microplastic accumulation in riverbed sediment via hyporheic exchange from headwaters to mainstems. Sci. Adv. 8 (2), eabi9305 https://doi.org/10.1126/sciadv.abi9305.

Eerkes-Medrano, D., Thompson, R.C., Aldridge, D.C., 2015. Microplastics in freshwater systems: a review of the emerging threats, identification of knowledge gaps and prioritisation of research needs. Water Res. 75, 63–82. https://doi.org/10.1016/j.watres.2015.02.012.

Enders, K., Lenz, R., Stedmon, C.A., Nielsen, T.G., 2015. Abundance, size and polymer composition of marine microplastics $\geq$ 10 Mm in the Atlantic Ocean and their modelled vertical distribution. Mar. Pollut. Bull. 100 (1), 70–81. https://doi.org/10.1016/j.marpolbul.2015.09.027.

Fan, P., Yu, H., Xi, B., Tan, W., 2022. A review on the occurrence and influence of biodegradable microplastics in soil ecosystems: are biodegradable plastics substitute or threat? Environ. Int. 163, 107244. https://doi.org/10.1016/j.envint.2022.107244.

Frei, S., Piehl, S., Gilfedder, B.S., Löder, M.G.J., Krutzke, J., Wilhelm, L., Laforsch, C., 2019. Occurence of microplastics in the hyporheic zone of rivers. Sci. Rep. 9 (1), 15256. https://doi.org/10.1038/s41598-019-51741-5.

Frias, J.P.G.L., Nash, R., 2019. Microplastics: finding a consensus on the definition. Mar. Pollut. Bull. 138, 145–147. https://doi.org/10.1016/j.marpolbul.2018.11.022.

Geissen, V., Mol, H., Klumpp, E., Umlauf, G., Nadal, M., Van Der Ploeg, M., Van De Zee, S.E.A.T.M., Ritsema, C.J., 2015. Emerging pollutants in the environment: a challenge for water resource management. Int. Soil Water Conserv. Res. 3 (1), 57–65. https://doi.org/10.1016/j.iswcr.2015.03.002.

Goharzadeh, A., Khalili, A., Jørgensen, B.B., 2005. Transition layer thickness at a fluid-porous interface. Phys. Fluids 17 (5), 057102. https://doi.org/10.1063/1.1894796.

Goharzadeh, A., Saidi, A., Wang, D., Merzkirc, W., Khalil, A., 2006. An experimental investigation of the brinkman layer thickness at a fluid-porous Interface. In: Meier, G.E.A., Sreenivasan, K.R., Heinemann, H.-J. (Eds.), IUTAM Symposium on One Hundred Years of Boundary Layer Research. In: Gladwell, G.M.L. (Ed.), Series Ed.; Solid Mechanics and its Applications, vol. 129. Springer Netherlands, Dordrecht, pp. 445–454. https://doi.org/10.1007/978-1-4020-4150-1_43.

Grant, S.B., Gomez-Velez, J.D., Ghisalberti, M., 2018a. Modeling the effects of turbulence on hyporheic exchange and local-to-global nutrient processing in streams. Water Resour. Res. 54 (9), 5883–5889. https://doi.org/10.1029/2018WR023078.

Grant, S.B., Azizian, M., Cook, P., Boano, F., Rippy, M.A., 2018b. Factoring stream turbulence into global assessments of nitrogen pollution. Science 359 (6381), 1266–1269. https://doi.org/10.1126/science.aap8074.

Han, X., Fang, H., He, G., Reible, D., 2018. Effects of roughness and permeability on solute transfer at the sediment water interface. Water Res. 129, 39–50. https://doi.org/10.1016/j.watres.2017.10.049.

Han, X., Fang, H.W., Johnson, M.F., Rice, S.P., 2019. The impact of biological bedforms on near-bed and subsurface flow: a laboratory-evaluated numerical study of flow in

the vicinity of pits and mounds. Case Rep. Med. 124 (7), 1939–1957. https://doi.org/10.1029/2019JF005000.
Horton, A.A., Dixon, S.J., 2018. Microplastics: an introduction to environmental transport processes. WIREs Water 5 (2). https://doi.org/10.1002/wat2.1268.
Issac, M.N., Kandasubramanian, B., 2021. Effect of microplastics in water and aquatic systems. Environ. Sci. Pollut. Res. 28 (16), 19544–19562. https://doi.org/10.1007/s11356-021-13184-2.
Karkanorachaki, K., Syranidou, E., Kalogerakis, N., 2021. Sinking characteristics of microplastics in the marine environment. Sci. Total Environ. 793, 148526. https://doi.org/10.1016/j.scitotenv.2021.148526.
Kazezyılmaz-Alhan, C.M., Medina, M.A., 2006. Stream solute transport incorporating hyporheic zone processes. J. Hydrol. 329 (1–2), 26–38. https://doi.org/10.1016/j.jhydrol.2006.02.003.
Lambert, S., Wagner, M., 2018. Microplastics Are Contaminants of Emerging Concern in Freshwater Environments: An Overview. Springer International Publishing.
Laursen, S.N., Fruergaard, M., Dodhia, M.S., Posth, N.R., Rasmussen, M.B., Larsen, M.N., Shilla, D., Shilla, D., Kilawe, J.J., Kizenga, H.J., Andersen, T.J., 2023. Settling of buoyant microplastic in estuaries: the importance of flocculation. Sci. Total Environ. 886, 163976. https://doi.org/10.1016/j.scitotenv.2023.163976.
Lewandowski, J., Arnon, S., Banks, E., Batelaan, O., Betterle, A., Broecker, T., Coll, C., Drummond, J., Gaona Garcia, J., Galloway, J., Gomez-Velez, J., Grabowski, R., Herzog, S., Hinkelmann, R., Höhne, A., Hollender, J., Horn, M., Jaeger, A., Krause, S., Löchner Prats, A., Magliozzi, C., Meinikmann, K., Mojarrad, B., Mueller, B., Peralta-Maraver, I., Popp, A., Posselt, M., Putschew, A., Radke, M., Raza, M., Riml, J., Robertson, A., Rutere, C., Schaper, J., Schirmer, M., Schulz, H., Shanafield, M., Singh, T., Ward, A., Wolke, P., Wörman, A., Wu, L., 2019. Is the hyporheic zone relevant beyond the scientific community? Water 11 (11), 2230. https://doi.org/10.3390/w11112230.
Li, J., Liu, H., Paul Chen, J., 2018. Microplastics in freshwater systems: a review on occurrence, environmental effects, and methods for microplastics detection. Water Res. 137, 362–374. https://doi.org/10.1016/j.watres.2017.12.056.
Li, C., Busquets, R., Campos, L.C., 2020. Assessment of microplastics in freshwater systems: a review. Sci. Total Environ. 707, 135578. https://doi.org/10.1016/j.scitotenv.2019.135578.
Lian, Y.P., Dallmann, J., Sonin, B., Roche, K.R., Liu, W.K., Packman, A.I., Wagner, G.J., 2019. Large Eddy simulation of turbulent flow over and through a rough permeable bed. Comput. Fluids 180, 128–138. https://doi.org/10.1016/j.compfluid.2018.12.015.
Lian, Y.P., Dallmann, J., Sonin, B., Roche, K.R., Packman, A.I., Liu, W.K., Wagner, G.J., 2021. Double averaging analysis applied to a large eddy simulation of coupled turbulent overlying and porewater flow. Water Resour. Res. 57 (11) https://doi.org/10.1029/2021WR029918.
Ling, X., Yan, Z., Lu, G., 2022. Vertical transport and retention behavior of polystyrene nanoplastics in simulated hyporheic zone. Water Res. 219, 118609. https://doi.org/10.1016/j.watres.2022.118609.
Lu, L., Luo, T., Zhao, Y., Cai, C., Fu, Z., Jin, Y., 2019. Interaction between microplastics and microorganism as well as gut microbiota: a consideration on environmental animal and human health. Sci. Total Environ. 667, 94–100. https://doi.org/10.1016/j.scitotenv.2019.02.380.
Luo, H., Xiang, Y., He, D., Li, Y., Zhao, Y., Wang, S., Pan, X., 2019. Leaching behavior of fluorescent additives from microplastics and the toxicity of leachate to chlorella vulgaris. Sci. Total Environ. 678, 1–9. https://doi.org/10.1016/j.scitotenv.2019.04.401.
Manes, C., Pokrajac, D., McEwan, I., Nikora, V., 2009. Turbulence structure of open channel flows over permeable and impermeable beds: a comparative study. Phys. Fluids 21 (12), 125109. https://doi.org/10.1063/1.3276292.
Mangan, M.R., Oldroyd, H.J., Paw .K.T., U, Clay, J.M., Drake, S.A., Kelley, J., Suvočarev, K., 2022. Integrated quadrant analysis: a new method for analyzing turbulent coherent structures. Bound.-Layer Meteorol. 184 (1), 45–69. https://doi.org/10.1007/s10546-022-00694-w.
Moin, P., Kim, J., 1982. Numerical investigation of turbulent channel flow. J. Fluid Mech. 118 (1), 341. https://doi.org/10.1017/S0022112082001116.
Molazadeh, M., Liu, F., Simon-Sánchez, L., Vollersten, J., 2023. Buoyant microplastics in freshwater sediments – how do they get there? Sci. Total Environ. 860, 160489. https://doi.org/10.1016/j.scitotenv.2022.160489.
Ng, K.L., Obbard, J.P., 2006. Prevalence of microplastics in Singapore's coastal marine environment. Mar. Pollut. Bull. 52 (7), 761–767. https://doi.org/10.1016/j.marpolbul.2005.11.017.
Nizzetto, L., Bussi, G., Futter, M.N., Butterfield, D., Whitehead, P.G., 2016. A theoretical assessment of microplastic transport in river catchments and their retention by soils and river sediments. Environ Sci Process Impacts 18 (8), 1050–1059. https://doi.org/10.1039/C6EM00206D.
Osorio, E.D., Tanchuling, M.A.N., Diola, Ma.B.L.D., 2021. Microplastics occurrence in surface waters and sediments in five river mouths of Manila Bay. Front. Environ. Sci. 9, 719274. https://doi.org/10.3389/fenvs.2021.719274.
Peng, G., Xu, P., Zhu, B., Bai, M., Li, D., 2018. Microplastics in freshwater river sediments in Shanghai, China: a case study of risk assessment in mega-cities. Environ. Pollut. 234, 448–456. https://doi.org/10.1016/j.envpol.2017.11.034.
Qiu, Q., Peng, J., Yu, X., Chen, F., Wang, J., Dong, F., 2015. Occurrence of microplastics in the coastal marine environment: first observation on sediment of China. Mar. Pollut. Bull. 98 (1–2), 274–280. https://doi.org/10.1016/j.marpolbul.2015.07.028.
Rodi, W., 2010. Large eddy simulation of river flows. In: Proceedings of the International Conference on Fluvial Hydraulics. Bundesanstalt fur Wasserbau, Karlsruhe, Germany, pp. 23–32.
Rodríguez-Narvaez, O.M., Goonetilleke, A., Perez, L., Bandala, E.R., 2021. Engineered technologies for the separation and degradation of microplastics in water: a review. Chem. Eng. J. 414, 128692. https://doi.org/10.1016/j.cej.2021.128692.
Schmidt, C., Krauth, T., Wagner, S., 2017. Export of plastic debris by rivers into the sea. Environ. Sci. Technol. 51 (21), 12246–12253. https://doi.org/10.1021/acs.est.7b02368.
Schmidt, N., Thibault, D., Galgani, F., Paluselli, A., Sempéré, R., 2018. Occurrence of microplastics in surface waters of the Gulf of Lion (NW Mediterranean Sea). Prog. Oceanogr. 163, 214–220. https://doi.org/10.1016/j.pocean.2017.11.010.
Serra, T., Colomer, J., 2023. Scavenging of polystyrene microplastics by sediment particles in both turbulent and calm aquatic environments. Sci. Total Environ. 884, 163720. https://doi.org/10.1016/j.scitotenv.2023.163720.
Shahiri Tabarestani, E., Afzalimehr, H., Pham, Q.B., 2021. Validation of double averaged velocity method in a variable width river. Earth Sci. Inform. 14 (4), 2265–2278. https://doi.org/10.1007/s12145-021-00692-5.
Shen, G., Yuan, J., Phanikumar, M.S., 2022. Quantifying the effects of bed roughness on transit time distributions via direct numerical simulations of turbulent hyporheic exchange. Water Resour. Res. 58 (4) https://doi.org/10.1029/2021WR030503.
Spalart, P., Jou, W.-H., Strelets, M., Allmaras, S., 1997. Comments on the Feasibility of LES for Wings, and on a Hybrid RANS/LES Approach.
Spalart, P.R., Deck, S., Shur, M.L., Squires, K.D., Strelets, M.Kh., Travin, A., 2006. A new version of detached-eddy simulation, resistant to ambiguous grid densities. Theor. Comput. Fluid Dyn. 20 (3), 181–195. https://doi.org/10.1007/s00162-006-0015-0.
Summers, E., Du, J., Park, K., Kaiser, K., 2023. How does buoyancy behavior impact microplastic transport in an estuarine environment? Sci. Total Environ. 899, 165687. https://doi.org/10.1016/j.scitotenv.2023.165687.
Tsai, C.W., Huang, S., 2019. Modeling suspended sediment transport under influence of turbulence ejection and sweep events. Water Resour. Res. 55 (7), 5379–5393. https://doi.org/10.1029/2018WR023493.
Van Wijnen, J., Ragas, A.M.J., Kroeze, C., 2019. Modelling global river export of microplastics to the marine environment: sources and future trends. Sci. Total Environ. 673, 392–401. https://doi.org/10.1016/j.scitotenv.2019.04.078.
Wagner, M., Scherer, C., Alvarez-Muñoz, D., Brennholt, N., Bourrain, X., Buchinger, S., Fries, E., Grosbois, C., Klasmeier, J., Marti, T., Rodriguez-Mozaz, S., Urbatzka, R., Vethaak, A.D., Winther-Nielsen, M., Reifferscheid, G., 2014. Microplastics in freshwater ecosystems: what we know and what we need to know. Environ. Sci. Eur. 26 (1), 12. https://doi.org/10.1186/s12302-014-0012-7.
Waldschläger, K., Schüttrumpf, H., 2019. Effects of particle properties on the settling and rise velocities of microplastics in freshwater under laboratory conditions. Environ. Sci. Technol. 53 (4), 1958–1966. https://doi.org/10.1021/acs.est.8b06794.
Waldschläger, K., Born, M., Cowger, W., Gray, A., Schüttrumpf, H., 2020. Settling and rising velocities of environmentally weathered micro- and macroplastic particles. Environ. Res. 191, 110192. https://doi.org/10.1016/j.envres.2020.110192.
Wallace, J.M., 2016. Quadrant analysis in turbulence research: history and evolution. Annu. Rev. Fluid Mech. 48 (1), 131–158. https://doi.org/10.1146/annurev-fluid-122414-034550.
Wallace, J.M., Eckelmann, H., Brodkey, R.S., 1972. The wall region in turbulent shear flow. J. Fluid Mech. 54 (1), 39–48. https://doi.org/10.1017/S0022112072000515.
Wang, W., Ndungu, A.W., Li, Z., Wang, J., 2017. Microplastics pollution in inland freshwaters of China: a case study in urban surface waters of Wuhan, China. Sci. Total Environ. 575, 1369–1374. https://doi.org/10.1016/j.scitotenv.2016.09.213.
Wang, C., Briggs, M.A., Day-Lewis, F.D., Slater, L.D., 2021. Characterizing physical properties of streambed interface sediments using in situ complex electrical conductivity measurements. Water Resour. Res. 57 (2), e2020WR027995 https://doi.org/10.1029/2020WR027995.
Yang, L., Zhang, Y., Kang, S., Wang, Z., Wu, C., 2021. Microplastics in freshwater sediment: a review on methods, occurrence, and sources. Sci. Total Environ. 754, 141948. https://doi.org/10.1016/j.scitotenv.2020.141948.
Zhou, T., Endreny, T.A., 2013. Reshaping of the hyporheic zone beneath river restoration structures: flume and hydrodynamic experiments: HYPORHEIC EXCHANGE BENEATH RIVER RESTORATION STRUCTURES. Water Resour. Res. 49 (8), 5009–5020. https://doi.org/10.1002/wrcr.20384.